Engineering Geology 194 (2015) 12–24

Contents lists available at ScienceDirect

Engineering Geology

journal homepage: www.elsevier.com/locate/enggeo

Evaluation of landslide mechanisms characterized by high-speed mass ejection and long-run-out based on events following the Wenchuan earthquake

Hui-Ming Tang [a], Xiao Liu [a,b,*], Xin-Li Hu [a], D.V. Griffiths [b]

[a] Three Gorges Research Center for Geo-hazards of Ministry of Education, China University of Geosciences, Wuhan 430074, China
[b] Department of Civil and Environmental Engineering, Colorado School of Mines, Golden, CO 80401, United States

ARTICLE INFO

Article history:
Received 3 August 2013
Received in revised form 30 December 2014
Accepted 8 January 2015
Available online 14 January 2015

Keywords:
Landslide
High-speed and long-run-out
Seismic hazard
Formation mechanism
Reliability analysis
Wenchuan earthquake

ABSTRACT

In the 2008 Wenchuan earthquake, the mass ejection type of high-speed and long-run-out landslide was an unusual hazard characterized by its dramatic phenomenon of a huge slope mass launching into the air and becoming airborne for a long distance. Quantitative and qualitative combined techniques were applied to reveal the formation mechanism of this type of landslide. Four prerequisites critical to form mass ejection are identified: high position of the toe of the surface of rupture, critical height and critical inclination of slope, sufficient open space in the movement direction, and adequate take-off speed of ski-jump-like mass ejection. These four area-specific prerequisites provide a promising approach for screening and targeting the potential landslides. Subsequently, a dynamic reliability analysis method that considers the feature of energy–time distribution is proposed. This site-specific method provides a more credible evaluation by emphasizing the most significant period within the whole earthquake duration. Finally, an aerodynamic inverse method combined with an energy-conservation-based method is applied in the quantitative evaluation to calculate take-off speed of mass ejection. This paper provides a viable solution for regional screening and site assessment for new potential targets of this type of landslide.

1. Introduction

Earthquake-induced landslides frequently cause the most extensive damage as demonstrated in the 2008 Wenchuan earthquake in which earthquake-induced landslides were among the major geological disasters. In these landslides (e.g., Cui et al., 2012; Guo and Hamada, 2013; Liu et al., 2010; Qi et al., 2010, 2012; Tang et al., 2010, 2011a,b; Wang et al., 2009, 2013; Wu et al., 2012; Xu and Xu, 2012; Yin et al., 2009, 2011), there is an unusual type of landslide named "mass ejection type of high-speed and long-run-out" (ME-HSLR) landslide. This type of landslide is characterized by concealed development, sudden break-out, dramatic ejection of landslide material through the air, and devastating consequences. Generally, unlike rock avalanches, landslides have significantly more horizontal movement than vertical movement. However, this distinction is not absolute. Therefore, in a general sense this type of ME-HSLR landslide can be also described as rock avalanches with the feature of becoming airborne. The potential for development of such a landslide is hidden because of the slope's relatively high stability under normal static conditions. Routine slope stability assessment methods may not distinguish ME-HSLR from common potential landslides and often only high magnitude earthquakes reveal the hidden slope features that produce large-scale mass ejection, accompanied by its sudden occurrence, wider scope, and devastating consequences.

Why do only a small part of the earthquake-induced landslides distinguishes themselves by the dramatic character of mass ejection and what formation mechanism occurs in this type of landslide? Finding answers to these questions is the goal of this paper. The formation mechanism of this type of landslide is so unusual that it has not been well revealed before. Recent seismic activity producing catastrophic damage to populated areas around the world has presented new challenges to academia and it can be predicted that the ME-HSLR landslide will attract increased attention.

The overall framework of this paper consists of four parts that focus on the formation mechanism of this form of landslide. The first part utilizes engineering geology qualitative analysis on selected areas. Data collected from actual and typical cases in the Wenchuan area were used to analyze and discover the critical features that produce this type of landslide, and there exist four prerequisites to this type of landslide, which can be used as area-specific screening criteria that considerably narrow the selection of slopes likely to develop into ME-HSLR landslides. The second part focuses on quantitative assessment of the dynamic reliability of site-specific target landslides. A new reliability analysis method using energy–time distribution is proposed. The third part is dedicated to determining a value for the take-off speed of

* Corresponding author at: Three Gorges Research Center for Geo-hazards of Ministry of Education, China University of Geosciences, Wuhan 430074, China.
E-mail addresses: tanghm@cug.edu.cn (H.-M. Tang), liuxiao@cug.edu.cn (X. Liu), huxli2000@163.com (X.-L. Hu), d.v.griffiths@mines.edu (D.V. Griffiths).

http://dx.doi.org/10.1016/j.enggeo.2015.01.004
0013-7952/

landslide material that becomes airborne, which is a key element of this type of landslide. A new strategy that combines aerodynamic inverse procedure and energy-conservation-based forward method is suggested. As a verification, the fourth part provides a complete case study to carry out these new concepts and methods. Benefiting from the advantages of qualitative and quantitative methods as well as the combination of area-specific and site-specific procedures, the final analysis results are more reliable than previously used methods. The most important significance of this study is not the analysis of the past landslides, however, but rather its ability to analyze susceptibility for future landslides providing foresight that can lead to reduced loss of life and property.

2. Overview of mass ejection type of high-speed and long-run-out (HSLR) landslides induced by Wenchuan earthquake

The Wenchuan earthquake trigged over 56,000 landslides (Dai et al., 2011), but the most unusual form was the earthquake-induced HSLR landslide. Compared with non-earthquake triggered high-speed and long-run out landslides, such as the Yigong landslide (Wang, 2008) in China, those triggered by the earthquake often produced the significant feature of mass ejection.

According to statistics of previous studies, there are over 18 large-scale HSLR landslides and some of them have been relatively well studied (e.g., Fang, 2010; Liu et al., 2012; Wang et al., 2009; Wu et al., 2010; Yin, 2009; Yin et al., 2009, 2011). Tables 1 and 2 give the geological and motion characteristics overview respectively for 6 HSLR landslides which have the feature of mass ejection. These are the Jingu landslide (Liu et al., 2012), the Niujuangou landslide (Yin et al., 2011), the Donghekou landslide (Wang et al., 2009; Yin et al., 2009), the Daguangbao landslide (Huang et al., 2012; Yin et al., 2009), the Xiejiadianzi landslide (Wang et al., 2013; Yin et al., 2009), and the Chengxi landslide (Yin et al., 2009, 2011) as shown in Fig. 1.

3. Four prerequisites critical to mass ejection type of HSLR landslides

The landslide body's strong vibration caused by the earthquake is one of the main reasons, but not the only reason, for "mass ejection" of HSLR landslides. From the point of view of system theory, the earthquake is an external excitation outside the landslide system. By means of rock and soil mechanics as well as earthquake dynamics techniques, the impact of the earthquakes on the slope can be assessed quantitatively, which is illustrated in Section 4 of this paper. However, this type of site-specific analysis is very complex and requires a high density of high-quality rock and soil property data, an accurate dynamic model of rock and soil behavior, and accurate data of seismic loads (Jibson, 2011; Wasowski et al., 2011). Proper consideration of costs–benefits requires pre-screening of targets before undertaking expensive and time-consuming heavy-duty quantitative analysis.

Using engineering geological analysis, we can improve the efficiency of regional screening by identifying four prerequisites (commonalities) that are critical to the formation of ME-HSLR landslides.

Based on Tables 1 and 2, the four prerequisites are abstracted and listed below.

3.1. High position

The first prerequisite is high position of the landslide. The term "high position" does not refer to the height of the entire slope but describes the net vertical distance from the toe of the rupture surface down to the valley bottom. High position can ensure adequate distance of vertical drop from the toe of the rupture to valley bottom. From Table 2, a significant mass ejection often requires 0.3 km or more drop distance, and when the distance is lower than 0.3 km, the feature of mass ejection is not very significant. For example, although the Daguangbao landslides had a 0.7 km average vertical drop corresponding to a long average horizontal movement of 2.2 km, the vertical distance from the toe of the rupture surface to the valley bottom was only 0.2 km, which resulted in mass ejection comparing with the other landslides in Table 2. The same situation happened in the Chengxi landslide where the vertical drop from the toe of the rupture surface to valley bottom was only 0.15 km.

3.2. Critical height and critical inclination of slope

The second prerequisite is that the slope height and slope inclination should match a statistical relationship which was presented by Keefer (1984) for high speed and long runout avalanche. As shown in Table 1, it is noted that the average inclination is from 30 to 40° while the typical source slope height is from 250 to 600 m except for the case of 1300 m height of Daguangbao landslide. This indicator matches well with the finding by Keefer (1984). Therefore, for the purpose of locating potential HSLR landslides in Wenchuan area, we suggest that the critical slope height is 250 m while the critical slope inclination is 30°. This is an efficient way to screen the potential target landslides which have the ability to develop into HSLR landslides.

3.3. Sufficient open space in movement direction

The third prerequisite is sufficient open space in the front direction. If there is a capacious space in the movement direction of the landslide, the mass ejection will benefit from it. In contrast, a confined space will significantly reduce the development of mass ejection. For example, the movement of the Chengxi landslide (Yin et al., 2009, 2011) was impeded by large residential buildings located in the movement route. The Niujuangou landslide is another special HSLR landslide characterized by four impacts which resulted in a unique trajectory indicated by the five polylines (Yin et al., 2011). Although the movement of this landslide

Table 1
Landslides geological overview.

Landslides	Latitude and longitude	Transportation distance from the main fracture/km	Source slope height/m	Average surface gradient/°	Inclination relationship	Formation and lithology
Jingu	N31° 58′17″–58′27″ E104° 35′54″–36′24″	1.0	600	41	Bedding	Strong weathered, broken Cambrian slate and Silurian mudstone
Niujuangou	N31° 01′21″–03′16″ E103° 25′12″–28′31″	0.5	450	35	Bedding	Strong weathered, broken Archean granodiorite
Donghekou	N32° 24′17″–24′49″ E105° 006′21″–07′19″	4.0	600	31	Bedding	Strong weathered, broken Lower Cambrian carbonaceous slate, shale, sandstone, limestone
Daguangbao	N31° 37′53″–31° 39′13″ E104° 05′7″55″–08′23″	7.0	1300	55	Bedding	Fractured Permian and Triassic limestone, mudstone, shale
Xiejiadianzi	N31° 17′31″–18′16″ E103° 50′07″–50′53″	1.1	250	35	–	Proterozoic granite, gabbro, granodiorite with joint developed
Chengxi	N31° 49′40″–49′50″ E104° 26′57″–27′21″	0.3	300	40	Reversed	Strong weathered, broken Cambrian sandstone and shale

Table 2
Landslides motion characteristics overview.

Landslides	Vertical drop from toe of surface of rupture to valley bottom/km	Average distance of vertical movement/km	Average distance of horizontal movement/km	Proportional coefficient of horizontal movement	Take-off speed of mass ejection/m·s^{-1}	Feature of mass ejection	Feature of debris flows	Open space in movement direction
Jingu	0.30	0.40	0.7	2.3	75	Significant	Significant	Capacious
Niujuangou	0.40	0.50	3.2	8.0	70	Significant	Significant	Capacious
Donghekou	0.30	0.40	1.3	4.3	70	Significant	Significant	Capacious
Daguangbao	0.20	0.70	2.2	11.0	25	Medium	Medium	Capacious
Xiejiadianzi	0.70	0.80	1.5	2.1	72	Significant	Significant	Capacious
Chengxi	0.15	0.25	0.4	2.7	70	Medium	Portion	Medium

Note: The "proportional coefficient of horizontal movement" is defined as the ratio of "average distance of horizontal movement" to "vertical drop from toe of surface of rupture to valley bottom."

was seriously influenced by the valley terrain, there was still considerable open space between the toe of the surface of rupture and the first impact point. This feature allowed the first stage movement of the Niujuangou landslide to have a significant mass ejection.

When screening potential sites it can be difficult to judge whether open space in the movement direction is "sufficient," so to quantitatively define this term we introduce a new factor named "proportional coefficient of horizontal movement" which is the ratio of "average distance of horizontal movement" to "vertical drop from toe of surface of rupture to valley bottom." Based on the features of the 6 landslides in Table 2, this ratio is from 2.1 to 11.0, so we define open space in the movement direction to be "sufficient" if the proportional coefficient of horizontal movement exceeds 2.0.

3.4. Adequate take-off speed

The fourth prerequisite is adequate take-off speed of mass ejection of landslide. In this paper, the term "take-off speed" is exactly the speed when the landslide mass has moved a considerable distance and reaches the "ski jump", and at this speed, the slope mass is torn out from the mother body.

Faster speeds result in more horizontal distance achieved by airborne material. Only if the take-off speed is large enough will the landslide's movement produce a significant overflight zone of airborne material. Therefore, the take-off speed of mass ejection from the source region of the landslide has important implications on the ability of long-distance transportation of the HSLR landslide. According to statistical results of previous researches, listed in Table 2, mass ejection will be a significant feature when take-off speeds reach 50–70 m/s.

4. Dynamic reliability analysis method of landslide

The above four prerequisites can be used to efficiently screen for target landslides. Slopes that satisfy all four prerequisites are the most likely to produce ME-HSLR landslides in seismic conditions. However, this area-specific qualitative approach is relatively rough so a site-specific quantitative analysis is needed to provide a more certain dynamic reliability assessment of potential landslides in seismic conditions. The combination of qualitative and quantitative approaches makes the analysis results more reliable. This paper provides a feasible approach for assessing the probability of a ME-HSLR landslide.

4.1. Instantaneous dynamic stability analysis

The instantaneous dynamic stability analysis plays a fundamental role in the framework of the entire dynamic reliability analysis of landslides, and provides quantitative data for the following procedure. Because the stress in a landslide is constantly changing during the period of seismic load, every moment of the dynamic stress field reflects a unique instantaneous state of the landslide. Thus, a quantitative evaluation of instantaneous dynamic stability of a landslide can be achieved by means of a certain procedure that interprets the instantaneous stress field.

The core of instantaneous dynamic stability analysis is the location of the transient critical slip surfaces during the seismic period and the evaluation of their corresponding instantaneous factors of safety. This process extracts a series of stress fields of the landslide by equal interval sampling and searches within the fields for each critical slip surface and its corresponding factor of safety. The result is a time series of critical

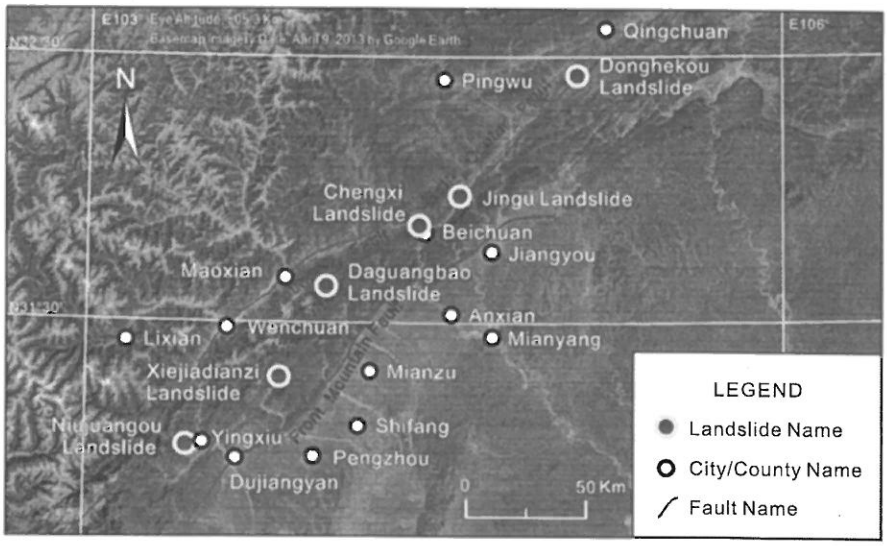

Fig. 1. Distribution of six typical high-speed and long-run-out landslides induced by Ms 8.0 Wenchuan earthquake.

slip surfaces and their time-histories of dynamic factors of safety. The specific steps are as follows:

(1) A numerical method is used (in this paper, FLAC3D is applied) to simulate the dynamic response of a landslide in the condition of seismic load. Then, a series of stress fields $StressField(i), i = 1,\cdots,N$ is obtained by sampling N times according to a certain fixed interval. The authors designed a program to generate the instantaneous stress fields by processing the exported raw data from the FLAC3D. Moreover, an interpolation algorithm proposed by Zheng et al. (2005) is involved in this program to improve the accuracy of each generated stress field.
(2) A polyline is used to represent the slip surface, non-circular slip surfaces are randomly generated, and Kulhawy's definition (1969) is applied to calculate the factor of safety of slip surfaces.

$$fos_{sl} = \left[\int_{sl} \tau_f ds\right] / \left[\int_{sl} \tau_{act} ds\right] \tag{1}$$

where sl represents the slip surface, fos_{sl} is the factor of safety, ds is the infinitesimal length of the slip surfaces, τ_f is soil shear strength, and τ_{act} is the actual shear stress in the location of ds.

(3) A multilayer particle swarm optimization technique is applied to drive the random generation process in step (2) to get non-circular slip surfaces (Liu, 2010; Liu and Ez Eldin, 2012), then the critical slip surface and its corresponding factor of safety is sought among all the random slip surfaces. The critical slip surface and its factor of safety can present the instantaneous response characteristics.
(4) For each stress field, steps (2) to (3) are repeated to obtain the time series of locations of instantaneous critical slip surfaces $\{Slide_i\}$ and the corresponding time series of instantaneous factors of safety $\{fos_i\}$, where, $i = 1,2\cdots n$.
(5) The $\{Slide_i\}$ and the corresponding $\{fos_i\}$ are the basic data for further dynamic reliability analysis of the potential landslide.

This method was proposed by the present authors and has been successfully applied in the Jingu landslide (Liu et al., 2012) with the feature of five advantages: (1) full nonlinear dynamic response analysis; (2) global optimization capabilities to locate the critical slip surfaces; (3) high-precision technique for stress field generation; (4) unique characteristics of non-circular and large degree of freedom regarding the performance of slip surface geometric; and (5) high-performance parallel computing capabilities.

4.2. Dynamic reliability analysis considering energy–time distribution

4.2.1. Limitation and simplification for the factors taken into account

In a given geometrical condition, four of the factors that influence the development and stability of landslides are: (1) landslide material's physico-mechanical properties, (2) randomness of variation in those properties, (3) dynamic changes of the material's physico-mechanical properties during seismic load, and (4) the characteristics of the seismic load. However, the magnitudes of the influences of the above listed factors are quite different. Actually, the critical slip surface and its factor of safety are functions of the stress field and physico-mechanical properties of material. In addition, the stress and the physico-mechanical properties all change with space and time, which causes the problem of dynamic landslide stability to become very complex. Fortunately, the degree of change of stress field is significantly higher than that of physico-mechanical properties during the whole dynamic load period so factor (3) has limited influence on the dynamic stability compared to factor (1) and (4). Additionally, factor (2) is relatively insignificant compared to factor (1).

The dynamic reliability analysis in this article is based on deterministic physico-mechanical properties of a landslide. Recognizing that the magnitudes of the influences of the above listed factors are quite different, and in pursuit of achieving progress in dynamic analysis methods, we focus on the most powerful influences and achieve considerable simplification of the analysis requirements by ignoring the secondary factors. The advantages of the progress achieved make the choice of simplification both acceptable and reasonable. Consequently, it is reasonable not to take account of the change of physico-mechanical properties during the period of dynamic load. It is also prudent, given the limits of current research knowledge, to reserve consideration of the randomness of the landslide's physico-mechanical properties for a later step in further research. Therefore, in this situation, the dynamic load caused by seismic energy is considered the only external excitation of the landslide system, so the dynamic reliability analysis in this paper is a direct reflection of the impact of the earthquake on the landslide.

Although there are some simplifications of the physico-mechanical properties, a new technique is proposed in this paper that introduces a statistical window of duration for reliability analysis based on quantitative analysis of energy–time distribution. Using a statistical window instead of whole duration can yield more credible results by emphasizing the most significant time period.

4.2.2. Mathematical model of reliability analysis

In general, probability of failure is defined as the probability that a structure or component cannot achieve its desired function. For slope stability, the landslide probability is the quantitative evaluation of the slope's instability from a probabilistic perspective. Both probability of failure and reliability index are the main quantitative evaluation indicators of this reliability analysis.

In landslide and slope reliability assessment (e.g., Christian et al., 1994; Dai et al., 2002), the limit state equation is shown as:

$$G(R,S) = G(\boldsymbol{X}) = Fos(\boldsymbol{X}) - K_T = 0 \tag{2}$$

where G is the performance function, R is the structural resistance, and S is the load effects. Specific to the slope stability problems, R and S can be generalized into vector $\boldsymbol{X}$, which contains various parameters affecting the landslide's stability, such as soil and rock layer physico-mechanical properties and dynamic loads. In this paper, material properties are constant values, and dynamic loads are variables in $\boldsymbol{X}$. $Fos(\boldsymbol{X})$ refers to the factor of safety. K_T is the threshold of the performance function and it often takes the constant value of 1 for landslide stability problems. If $G(\boldsymbol{X}) > 0$, the slope is stable; if $G(\boldsymbol{X}) < 0$, the slope will fail; if $G(\boldsymbol{X}) = 0$, the slope is in a state of limit equilibrium.

Therefore, the performance function $G(\boldsymbol{X})$ can be considered a safety margin, and the probability of failure can be defined as below (Xu and Low, 2006; Huang et al., 2010; Liu et al., 2013):

$$P_f = P[G(\boldsymbol{X}) \le 0] = \int_{G(X)\le 0} g(\boldsymbol{X}) dx \tag{3}$$

where P_f is the probability of failure and $g(\boldsymbol{X})$ is the joint probability density function of $G(\boldsymbol{X})$.

In addition, reliability index is introduced, which is defined as a ratio of the mathematical expectation of performance function and its standard deviation, as shown below.

$$\beta = \mu_G / \sigma_Z \tag{4}$$

where β is the reliability index, μ_G and σ_Z are the mathematical expectation and standard deviation of $G(\boldsymbol{X})$ respectively.

Considering that the dynamic factor of safety is a random process during seismic load, it can be described as a time-series $\{fos_i\}$, $i = 1,2\cdots n$. Accordingly, the time series of failure states are $\{S_i\}$, and each state can be calculated by Eq. (5) and the P_f can be obtained by Eq. (6) as below.

$$S_i = \begin{cases} 1, & fos_i \le 1 \\ 0, & fos_i > 1 \end{cases} \quad , \quad i = 1,2,\cdots,n \tag{5}$$

$$P_f = \frac{1}{n}\sum_{i=1}^{n} S_i \quad , \quad i = 1,2,\cdots,n. \tag{6}$$

In this procedure we obtained the P_f on the basis of the time-series $\{fos_i\}$, which is a useful way to discrete the time-based continuous variable. So, the Eq. (6) is a discretization form of Eq. (3).

4.2.3. Necessity of using statistical window of duration

Earthquake duration is defined as the total period from the arrival of the seismic waves to their disappearance (e.g., Bommer and Martinez-Pereira, 1999; Elnashai and Sarno, 2008; Housner, 1965). However, in most of this period, the vibration is at a relatively low level and has a limited impact on the landslide. The severe vibration, which has the greatest impact, usually accounts for only a small proportion of the total period. Although the significant period is short, it is crucial in its impact on the landslide stability. During this period, the factor of safety fluctuates strongly, and the instability is most likely to be triggered.

Previous literature (e.g., Liu et al., 2003) relating to the statistical analysis of dynamic factor of safety tended to use the entire earthquake duration. In other words, all the sampled dynamic factors of safety in time series $\{fos_i\}$ were included in the statistical process of Eqs. (5) to (6). However, the full period analysis is not the best way to reflect the characteristics of a dynamic system according to related theories of data mining and signal processing because the characteristics we should be concerned with may be overshadowed by the strong background noise in the full duration of the earthquake.

Rather than use the entire earthquake duration, we applied a statistical window of duration that covers the most severe vibration when performing the reliability analysis according to the method in Section 4.2.2. Therefore, only a subset of $\{fos_i\}$ corresponding to the statistical window of duration will be involved in the analysis. The application of the statistical window strengthens the utility of the results by emphasizing the most significant time period and eliminating irrelevant and non-significant time periods. In this way, the dilution effect on the statistical results is reduced and the reliability analysis yields more concise and credible results.

4.2.4. Statistical window of duration based on energy–time distribution analysis

Ground motion duration analysis (e.g., Elnashai and Sarno, 2008) is a powerful tool for insight into the energy–time distribution during a seismic event. Generally, the traditional ground motion duration analysis is based on the process of ground acceleration and is seldom designed for analyzing other response signals occurring during the seismic event. However, the concept and method can be extended to other related signals. Actually, the time-history of the dynamic factor of safety reflects the changing impact that an earthquake imposes on the landslide during the seismic event. Thus, it is feasible that the theories, concepts, and methods of well-developed ground motion duration analysis can migrate into the field of revealing characteristics of the dynamic factor of safety of landslides. In this paper, two new concepts named "accumulated energy of factor of safety" and "duration of factor of safety" are proposed and are aimed at the particular issue of energy–time distribution during the period of landslide dynamic response.

Because any fluctuation of signals contains energy, the concept of accumulated energy of factor of safety (AEF) is introduced in this paper with the definition as below:

$$AEF = \int_0^{Td} \Delta Fos^2(t)dt = \int_0^{Td} (Fos(t) - F_s)^2 dt \tag{7}$$

where AEF is accumulated energy of factor of safety, Td is earthquake duration, $Fos(t)$ is instantaneous factor of safety at the time t, F_s is static factor of safety, and $\Delta Fos(t)$ is the deviation between instantaneous factor of safety and static factor of safety.

The definition of AEF provides a theoretical foundation for acquisition of statistical windows of duration for the purpose of reliability analysis. The duration of factor of safety is defined as a certain time section of the AEF time curve in which an energy percentage range is appointed. For example, a 5%–95% range of AEF corresponds to start and end points of time, which bracket the duration of factor of safety. In this way, different assignments of energy range will result in various durations of factor of safety, which is set as the statistics windows for reliability analysis of dynamic landslide stability. The influence of selection of energy range will be discussed in detail in the case study.

5. Inverse method for calculating take-off speed of mass ejection

5.1. Necessity of using inverse method

The take-off speed of mass ejection of HSLR landslide has important implications on the ability of long-distance migration of substances within a landslide, so it has become one of the hot issues in this field. Because of the limitation of continuum theory of routine numerical simulation methods (e.g., finite-element and finite-difference), there exists an insurmountable obstacle to obtain the take-off speed of mass ejection. The velocities of element nodes in landslides during dynamic response present a different concept from the velocity of mass ejection. The former is a microscopic concept, which aims to characterize the reciprocating vibration of a discrete point in the landslide body. With the change of position, different points have different vibration velocities. The latter is a macro concept, and for simplicity's sake, the landslide is looked on as a whole object that has a uniform initial velocity. Therefore, the take-off speed of mass ejection cannot be simply the equivalent of a certain direct throw speed of the small-scale loose materials on the surface caused by seismic acceleration, but actually results from an upward thrust similar to a ski-jump from the toe of the surface of rupture.

Although researchers have suggested several forward methods (e.g., Hungr, 2004) to evaluate the take-off speed of mass ejection, using delivery distance to invert the take-off speed is the most viable option in the current research level. In fact, the aerodynamic theory and its inverse numerical methods have been able to answer the basic question of what take-off speed can ensure that the flying rigid body (or discrete bodies) will reach a certain delivery distance. Moreover, the aerodynamic-based inverse method is characterized by its high accuracy compared with soil-mechanics-based forward methods. For the purpose of landslide ejection velocity evaluation, a simplified inverse method can meet the analytical requirements.

5.2. Procedure of the inverse method

Because the huge sliding mass that is launched into the air is influenced in its movement by aerodynamic forces, it is sensible to analogize the sliding mass to the wing of an aircraft with similar aerodynamic implications and forces.

On the basis of summarized force analysis as shown in Fig. 2, Liu et al. (2002a) have studied the aerodynamic effects of the high-speed flying

of landslide body, and proposed a differential equation (Eq. (8)) for landslide gliding.

$$\left.\begin{aligned} F_L &= \frac{1}{2}G_e C_L(\alpha)\rho S\left[\left(\frac{dx}{dt}\right)^2+\left(\frac{dy}{dt}\right)^2\right] \\ F_R &= \frac{1}{2}C_R(\alpha)\rho S\left[\left(\frac{dx}{dt}\right)^2+\left(\frac{dy}{dt}\right)^2\right] \\ F_L\sin\phi - F_R\cos\phi &= m\frac{d^2x}{dt^2} \\ mg - F_L\cos\phi - F_R\sin\phi &= m\frac{d^2y}{dt^2} \\ \tan\varphi &= \frac{dy}{dx} \\ G_e &= S/H \end{aligned}\right\} \quad (8)$$

where F_L is lift force, F_R is resistance force; C_L is lift coefficient, C_R is resistance coefficient; ρ is the air density, t is time, H is sliding body's centroid height from the ground, S is wing area of sliding body, m is the mass of sliding body, and G_e is a dimensionless correction factor of ground effect on lift force.

As shown in Fig. 2, the positive direction of axis x is the horizontal direction of flight, positive direction of axis y is the direction of gravity, v is the velocity of centroid of sliding body, AB is a wing axis, ϕ is the angle between v and the positive direction of axis ox, and θ is the angle between AB and axis ox. When setting the positive direction of θ and ϕ as clockwise, the windward angle α, which is defined as the angle between v and AB, is $\alpha = \phi - \theta$.

According to wind tunnel tests (Liu et al., 2002b), the relationship between lift coefficient C_L, resistance coefficient C_R, and windward angle α as shown in Eq. (9).

$$\left.\begin{aligned} C_L(\alpha) &= 0.022\alpha - 0.002 \\ C_R(\alpha) &= C_L/(0.375\alpha - 0.375) \end{aligned}\right\}. \quad (9)$$

Although the analytical solution of the differential Eqs. (8) to (9) is difficult to obtain, it is easy to get numerical solutions. Based on the sliding body's centroid height from the ground H and the flight distance X, the inversion solution of the take-off speed of the mass ejection can be achieved.

6. Case study of Jingu HSLR landslide

Of all 6 landslides described in Tables 1 and 2, the Jingu landslide satisfies all 4 prerequisites critical to ME-HSLR landslides, making it a typical example of this type of landslide with the distinctive feature of mass ejection and the best choice for illustrating the formation mechanism of this type of landslide.

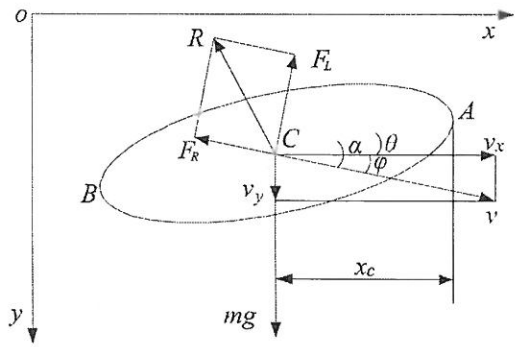

Fig. 2. Force sketch of gliding landslide body (after Liu et al., 2002a).

6.1. Engineering geology of Jingu landslide

6.1.1. Landslide profile

The Jingu landslide was located west of the Jingu Village, Chenjiaba Township, Beichuan County in Sichuan Province. The center location of the landslide body is N31°58′23.4″, E104°36′13.0″. The seismogenic fault (Beichuan–Yingxiu Fault), lies across the front of the landslide toe. The Wenchuan earthquake on 12th May 2008 triggered the Jingu landslide causing great devastation. The large mass ejection instantly covered the village along the flight path, causing heavy casualties. The perspective view of the landslide is shown in Fig. 3.

In order to reveal the formation mechanism of the Jingu landslide, the research team completed four field studies in this area since 2008 using engineering geological mapping, rock mechanics sampling, and geophysical field tests. The engineering geology plans and profile are shown in Figs. 3 and 4 respectively.

6.1.2. Landform feature and kinematic characteristic

The elevation of the crown of the Jingu landslide was over 1400 m, and the elevation of the valley under the toe of the landslide is 680 m. The height difference between the former and the latter is over 700 m, so the landslide has not only a huge potential energy but also a broad space for the release of potential energy.

The plane of the landslide is irregular, and its overall length is about 1200 m with the main slide direction SEE105°. Along the main axis of cross-section line AA′ in Fig. 4, the landslide consists of four parts: upper throwing depletion zone, lower sliding depletion zone, accumulation zone for secondary landslide mass, and accumulation zone for airborne mass. The zone classification and terminology reference the Cruden and Varnes (1996) and Varnes (1978). The upper throwing depletion zone is the source region (elevation from 1000 to 1300 m) where the huge mass that was launched into the air came from. This zone is characterized by the chair-back-like scarp and relatively flat slide bed. The take-off point (Point B, elevation 1000 m) of the airborne material is the toe of the surface of rupture, which divides the landslide into upper throwing depletion zone and lower sliding depletion zone. In the lower sliding depletion zone (elevation from 800 to 1000 m), the secondary-triggered landslide has formed a huge scarp. In the accumulation zone for secondary landslide mass (elevation from 700 to 800 m), the landslide formed a temporary dam that blocked the stream in front of the landslide toe. The accumulation zone for airborne mass (elevation from 740 m to 760 m) is located in the area surrounding the brickyard (elevation 740 m) and the roads (elevation 760 m). The airborne material flew over two zones, which are the lower sliding depletion zone and the accumulation zone for secondary landslide mass, and were deposited on the accumulation zone for airborne mass with max horizontal

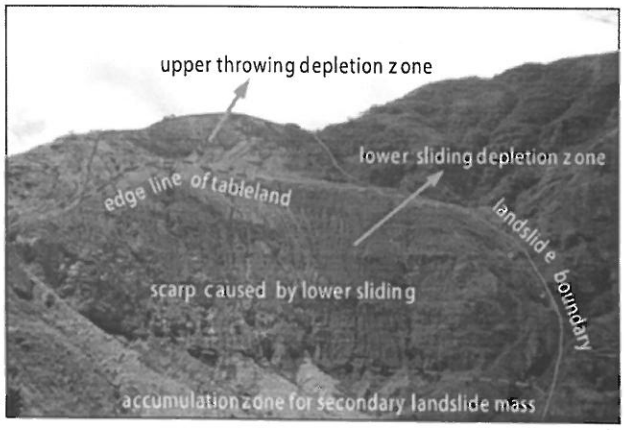

Fig. 3. Perspective view of Jingu high-speed and long-run-out landslide.

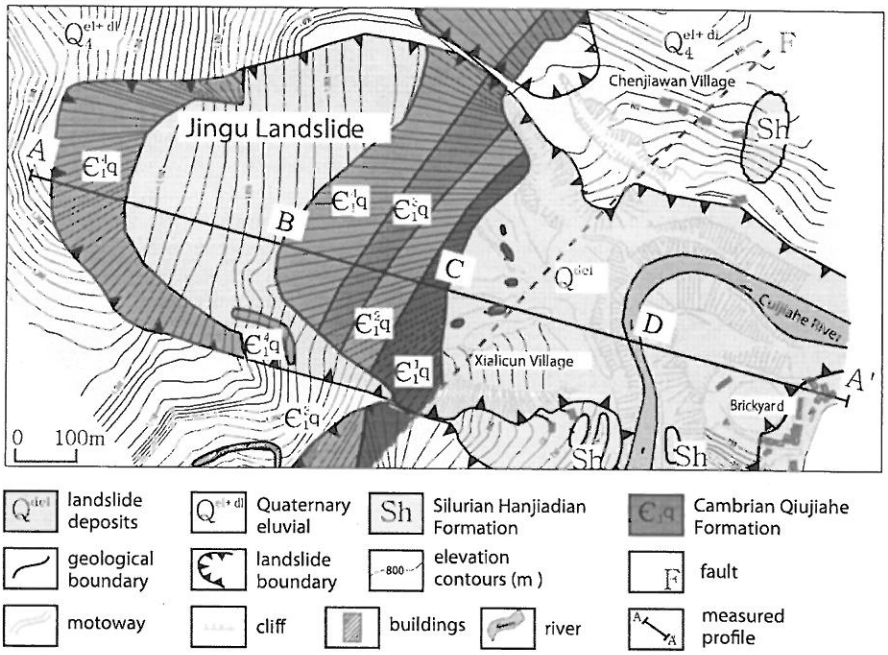

Fig. 4. Engineering geologic map of Jingu high-speed and long-run-out landslide.

transportation of 800 m. The lowest point of the over-flight area is located in the river (Point D, elevation 700 m).

Direct evidence confirmed the fact that during the subject landslides significant mass was launched into the air for a considerable airborne distance. After the landslide, homologous rock fragments of carbon siliceous slate with fresh traces of high-temperature carbonization appear in all four zones along the main axis, which indicates both the path of the landslide movement and the occurrence of high frictional heat conditions. If the landslide mass were transported by ground, the mass must flow along the surface from point A to point A′. The flowing mass would totally block the river (elevation 700 m) and then climb the south bank of the river to reach the brickyard and the roads (elevation 760 m). In this process, the river (Point D) would be seriously blocked with a thick layer (over 60 m) and would be much thicker than at the point A′. However, the investigation showed that the layer of rock fragments at accumulation zone for airborne mass (from point D to point A′) is obviously thicker than at point D. The fact that the river was just temporarily blocked, but not seriously, and it recovered naturally by the river flow itself, leads to the following two conclusions. First, that the river is the edge of the accumulation zone for secondary landslide mass, and second, that the main source of the thin-layer rock fragments located nearshore on the east bank of the river was material that separated and dropped from the greater mass that was flying over. All in all, the thickness distribution of the rock fragments is the direct measurable evidence and indicates the fact that the mass of upper throwing depletion zone launched into the air and became airborne for a considerable distance.

During the investigation in 2008, quite a few surviving residents who witnessed the event claimed that some part of the landslide mass was thrown over the river. The sky became dark and the hot wave of air with moisture blew people down, sometimes tearing off or shredding their clothes into pieces that were never found. This phenomenon is direct evidence of air blast from subsonic air displacement induced by the moving body of mass ejection. Many detailed records are filled with reports of this kind from seminars held between 2008 and 2010. Ultimately, the fact of the airborne mass of material was well documented and accepted by the surviving residents, investigators, and researchers.

6.1.3. Stratigraphy and lithology

The main exposed strata are Cambrian, Silurian and Quaternary. The boundary between the Cambrian and the Silurian is the Beichuan–Yinxiu Fault, whose hang wall is the Cambrian while the footwall is the Silurian. The strata are generally spread along the fault.

In the lower Cambrian Qiujiahe Formation, the main lithology is gray and black carbon siliceous slate with developed rock joints and fragment structures which result in low mechanics properties. This layer was mainly developed in the upper throwing area of the Jingu landslide. After the landslide, a lot of fragments of carbon siliceous slate remain on the stepped slip bed in the upper throwing area.

In the upper Silurian Hanjiadian Formation, the main lithology is argillite with weathered surface and fully developed structure planes which keep the rock in low mechanics properties. This layer was mainly exposed in the area to east bank of Cuijia River.

The lithology of Quaternary is mainly eluvium gravel soil which has a wide distribution as shown in Fig. 4.

6.1.4. Structure and earthquake

As shown in Fig. 1, the Jingu HSLR landslide is located in the Beichuan–Yinxiu Fault which is in the center of Longmenshan tectonic belt. This zone had significant activity in the Middle and Late Pleistocene. Since AD 638 years, the east edge region of Longmenshan experienced 66 Ms ≥ 4.7 earthquakes, and the biggest record is Ms 8.0 Wenchuan earthquake.

6.1.5. Hydrogeological conditions

The occurrence of groundwater in the study area can be divided into two forms: pore water and bedrock fissure water. The pore water occurs in the Quaternary loose deposits which are mainly distributed in accumulated areas of the slopes. The pore water is recharged by rainfall and fissure water in bedrock, and discharges into low—lying areas of gullies or infiltrates into bedrock fissures.

Fissure water is stored in fractured bedrock of Cambrian strata, and its storage is controlled by lithology and fracture development. In the central part of the scarp formed by the Jingu landslide, several small spring flows have developed.

6.2. Qualitative analysis of the formation mechanism of Jingu landslide

6.2.1. Formation mechanism

As shown in Figs. 3 and 5, The Jingu landslide is step-shaped, which divides the whole landslide into an upper and lower part. The upper part is the upper throwing depletion zone, while the lower part is the lower sliding depletion zone. On 700 to 750 meter elevation the landslide toe area is covered by a large amount of loose debris. On 800 to 1000 meter elevation is the scarp formed by the secondary-triggered landslide (sub-landslide). A gentle slope characterizes the 1000 to 1050 meter elevation. The upper and lower boundary is indicated by edge line of tableland in Fig. 3, which is the location of the toe of the surface of rupture. The upper throwing depletion zone extends from the toe of the surface of the rupture up to the crown of the landslide and has an elevation range of 1000–1300 m with the height of 300 m, width of 400 m, and length of 400 m. The total volume is about $2 \times 106\ m^3$.

During the earthquake, the slope mass of the upper throwing depletion zone was sheared and torn from the main body of the landslide, and the huge mass was launched from the location of the upper and lower boundary. After flying several hundred meters, the ejected mass seriously impacted the area across the river, and formed a huge area of debris splash.

The tableland edge line is not only the toe of the rupture surface of the upper part, but also the boundary between the upper part and the lower part of the landslide. The lower part was intensely scraped by the upper part. Combined with the effects from the upper part of the landslide and the earthquake activities, the lower part of the landslide was triggered into a secondary failure. The scarp in Fig. 3 is the remains of the secondary failure. Compared with the long-run-out movement of the upper part, the lower part had a relatively limited transport distance of 300 m. Most of the accumulated mass from the secondary landslide was distributed in the area near the west bank of the river.

According to the measured topography and field survey, the vertical drop from the toe of the rupture surface to valley bottom is over 300 m. At this height, the maximum horizontal distance of mass ejection is over 1000 m.

6.3. Dynamic reliability analysis

6.3.1. Model generalization and its parameters

The Jingu landslide has significantly changed the landform in the area. By comparing the original topographic maps before the earthquake and the engineering geological mapping data after the earthquake, and using information from interviews of local villagers, the research team set up the numerical model for simulation. In this model, as shown in Figs. 5 and 6, the boundary of the upper-layer-weathered charcoal siliceous slate and underlying lower-layer-slightly-weathered rock was deduced based on the result of rock acoustic velocity test.

Different from the static model, whose mesh density can be less dense in the non-core area in order to improve computation efficiency, the dynamic model should keep a high density mesh in the entire calculation area in order to minimize the impact on the model from high frequency components of the dynamic loads. So, the entire area of the model takes a high density mesh, as shown in Fig. 6.

In order to obtain the physico-mechanical properties of the Jingu landslide, various testing methods, including laboratory rock mechanics test, in situ field testing, and geophysical prospecting testing, were carried out. In addition, the engineering geological analogy was performed with the Xianfeng landslide in Wenchuan Earthquake area of Sichuan province (Liu et al., 2012). Each layer's physico-mechanical properties of the Jingu landslide are shown in Table 3. It is noted that we applied relatively low strength parameters, which approach residual strength, in the dynamic simulation and do not consider the change of these parameters with time. A more accurate method would use dynamic strength parameters in dynamic simulation; however, such an approach requires costly and time-consuming acquisition of the material's experimental dynamic parameters as well as significant progress of program codes. Considering these efforts beyond the scope of this paper, we must choose a certain simplification – fixing the strength parameters which approach residual strength. This simplification is reasonable at present research level because the change of physico-mechanical properties is significantly lower than the change of stress field during the whole dynamic load period.

The input seismic load is of the Wenchuan Earthquake record sampled by Chengdu Station No. 2 (in Chengdu City) which was set up before the earthquake and operated by China Earthquake Administration. Because the Jingu landslide is located in wilderness and sparsely populated, there is no station located exactly on it. However, the record of Chengdu Station No. 2 provides an alternate solution as accurately as possible considering the distance from the all available stations to the Jingu landslide. As shown in Fig. 7(a) and (b), the seismic load is synthesized with three components that correspond to three-dimensional

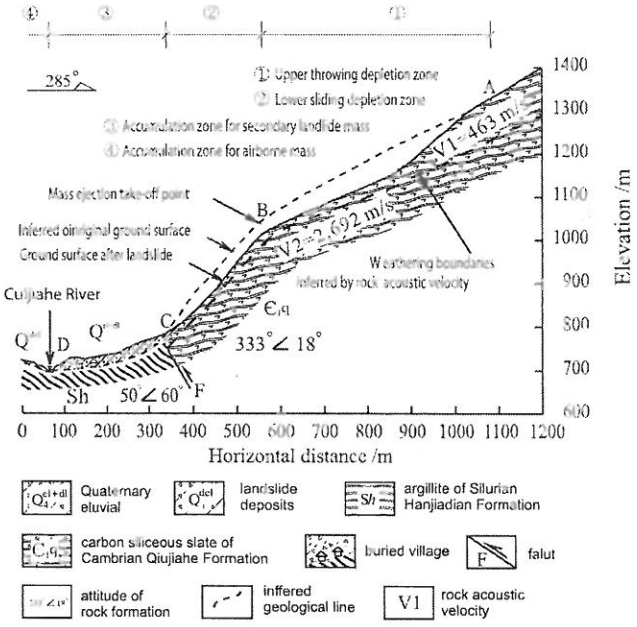

Fig. 5. Engineering geologic profile of Jingu high-speed and long-run-out landslide.

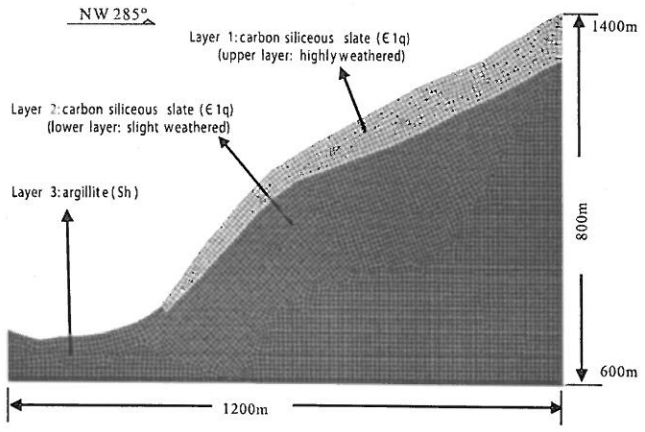

Fig. 6. Mesh generation of Jingu high-speed and long-run-out landslide.

Table 3
Mechanical properties of the layer of Jingu high-speed and long-run-out landslide.

Layers	Stratum	Lithology	Cohesion c/kPa	Friction φ/(°)	Density ρ/(kg·m^{-3})	Young's modulus E/MPa	Poisson's ratio/ν
1	Cambrian Qiujiahe Formation	Carbon siliceous slate (high weather)	300	25	2100	500	0.25
2	Cambrian Qiujiahe Formation	Carbon siliceous slate (slightly weather)	400	28	2200	700	0.25
3	Silurian Hanjiadian Formation	Argillite	50	40	1680	400	0.35

coordinates. The "BHE", "BHN" and "BHZ" are the three channels of the seismograph which represent the Cartesian components of three-directional space. The China Earthquake Administration gave these unified names to mark the direction of the data records. In X axis (the positive direction is NW285°), two horizontal waveforms from BHE channel (the positive direction is from West to East) and BHN channel (the positive direction is from South to North) were synthesized. In Z axis (the positive direction is upward), the vertical waveform of BHZ channel was applied. The Dynamic analysis parameters are listed in Table 4.

6.3.2. Time-history analysis of instantaneous factor of safety

Under dynamic conditions, the locations of instantaneous critical slip surfaces are significantly different from the static circumstance. In this case study, 180 s of the main shock of the Wenchuan earthquake were put into the numerical model, and 1441 instantaneous stress fields were obtained according to the sampling rate of 8 Hz. Each stress field was analyzed according to the method described in Section 4.1. In this way, 1441 instantaneous critical slip surfaces and their corresponding factors of safety were obtained. The 1441 data points constituted a time-history curve shown in Fig. 7(c), in which the maximum value is 1.17, the minimum value is 0.951, and the average value is 1.031. As a comparison, the static factor of safety is 1.037. In addition, all of the 1441 instantaneous critical slip surfaces were not uniformly distributed but were noticeably gathered into two clusters. Fig. 8 shows five critical slip surfaces among 1441 surfaces. It is noted that the static FOS value of 1.037 actually reflects the stability in residual strength condition because relatively low strength parameters, which approach residual strength, were applied in the dynamic simulation. That means the actual static stability of Jingu landslide before Wenchuan earthquake should be higher than 1.037.

6.3.3. Spatial distribution of dynamic critical slip surfaces

As shown in Fig. 8, two clusters of critical slip surfaces were developed and are marked with No. 1 and No. 2 respectively. The cluster No. 1 is located in the front part of the whole landslide, while cluster No. 2 is developed in the terrace on the middle-behind part of the whole landslide with the elevation from 1000 m to 1050 m. The tails of the two clusters have a certain overlap, however, the positions of the toes of their rupture surfaces have a significant difference.

6.3.4. Trigger mechanism of failure

Two sliding clusters mean three failure modes during the earthquake. The reason for the appearance of two sliding clusters lies mainly with the special combined effect of topography and lithology. The upper layer of the landslide is the weathered charcoal siliceous slate which has poor mechanical properties and the relatively gentle slope on the elevation of 1000 m provide a combination that makes it possible for the upper-body failure to be thrown out of the main body.

The so-called instantaneous instability refers to the state in which the factor of safety of a certain slip surface is reduced to less than 1.0 in a short time. It is widely accepted that instantaneous instability of a certain slip surface does not necessarily mean the landslide will fail along this slip surface. The reason for this phenomenon lies in the fact that any landslide's failure process takes time, namely progressive failure, and the instantaneous instability slip surface is often "fixed" and "submerged" by the rapidly changing stress state.

During dynamic loading, two factors apply to the instantaneous critical slip surface. First, its factor of safety is at a low level within a period of time, and second, its location is concentrated into a narrow range. We call the two factors a dual characteristic of the failure process. From the point of view of material mechanics, the values of these two factors reveal the extent to which, at a micro level, the slip surface material has suffered fatigue damage and strength deterioration. It is widely accepted that the micro level effect is progressive with time and will finally result in failure at the macro level. In addition, it is presently known that certain earthquake induced effects extremely accelerate the process of progressive failure. For example, the process of fatigue damage generates huge amounts of heat within a short period of time. This causes local vaporization of moisture that significantly increase pore pressure and reduce friction along the potential rupture surface (e.g., Campbell, 1989; Cleary and Campbell, 1993; Ersmann, 1979; Shreve, 1968), and as a result, the stability of the landslide is rapidly deteriorating.

According to the aforementioned dual characteristic of the failure process, the complexity of the Jingu landslide is such that the critical slip surfaces were not concentrated into just one cluster, but were divided into two clusters. Two clusters of critical slip surfaces in seismic condition will present three possible combinations of failure mode: single cluster No. 1, single cluster No. 2, or simultaneous failure of No. 1 and cluster No. 2. From the point of view of the random character of seismic condition, each failure mode can happen with a certain possibility. However, from the point of view of engineering geological conditions, we have concluded that the cluster No. 2 is more likely to dominate the failure than the other two modes. The four reasons for the higher probability of the cluster No. 2 failure are listed below:

First, the peak ground motion of cluster No. 2 is higher than the cluster No. 1 due to slope amplification effect. The location of cluster No. 2 is much higher and closer to the surface of the slope than that of the cluster No. 1, which resulted in higher amplification effect during the earthquake. The experimental research of Zhao et al. (2012), also shows that the failure near the surface has higher priority than depth damage of slope during seismic loading.

Second, the upper material of the slope is much more fractured than the lower, which results in low mechanical properties as shown in Table 3.

Table 4
Dynamic analysis parameters for Jingu high-speed and long-run-out landslide.

Boundary conditions			Dynamic load					Baseline correction and filtering	
Bottom	Left and right	Upper	Horizontal (NW285°)	Vertical	Interception duration/s	Waveform start time (UTC + 8)	Damping type	Filter type	Baseline correction polynomial type
Silent boundary	Free field boundary	Un-constrained	BHE + BHN channels orthogonal synthesis	BHZ channel	0–180	20080512 14:28:04.00	Local 0.5%π	Butterworth (0.1–5.0) Hz	Linear

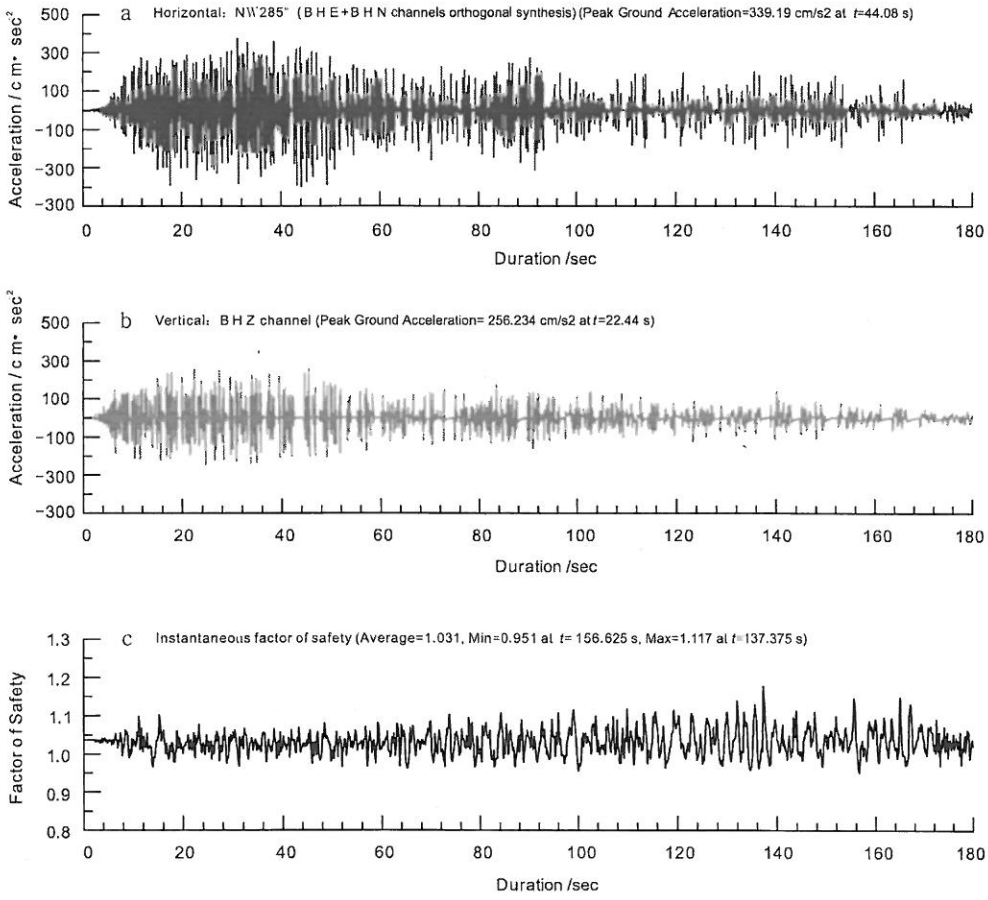

Fig. 7. Comparison of time-history curves of instantaneous factor of safety of Jingu high-speed and long-run-out landslide with the corresponding input Wenchuan earthquake waveform sampled by Chengdu Station No. 2 (CD2). (a) Horizontal: NW285° (BHE + BHN channels orthogonal synthesis) (peak ground acceleration = 399.19 cm/s^2 at t = 44.08 s); (b) Vertical: BHZ channel (peak ground acceleration = 256.234 cm/s^2 at t = 22.44 s); (c) Instantaneous factor of safety (Average = 1.031, Min = 0.951 at t = 156.625 s, Max = 1.117 at t = 137.375 s).

Third, the length of slip surfaces in cluster No. 2 is significantly shorter than that of cluster No. 1, which supports the assumption that the former has more possibility than the latter to lead to the failure of the landslide. Generally, the length of cluster No. 2 is approximately half the length of the cluster No. 1, and part of its tail coincides with the cluster No. 1. Even in strong earthquake conditions, as a landslide evolves it is impossible for a potential slip surface to achieve the plastic state zone completely connected within a short period of time. The most likely scenario is that the cluster No. 2 already experienced failure when the cluster No. 1 failure was still in development because the much shorter slip surface tends to achieve the failure state faster under the same conditions.

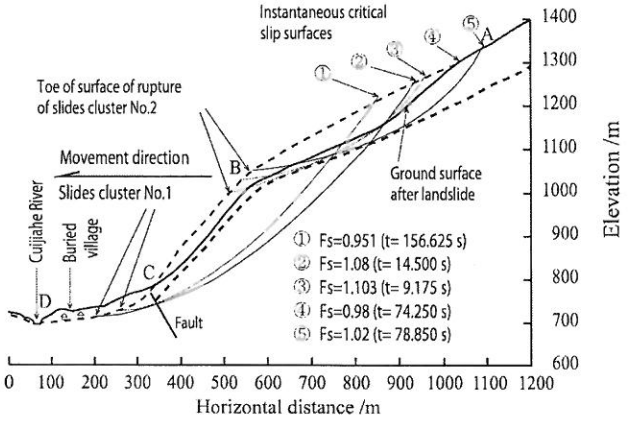

Fig. 8. Spatial distribution of the most dangerous slip surfaces of Jingu high-speed and long-run-out landslide.

Fourth, the domination failure mode of the cluster No. 2 will affect and change the separate development path of cluster No. 1. It is possible that two kinds of failure modes are both in development. However, once a failure occurs, the physico-mechanical conditions and the boundary conditions will change dramatically, therefore, the preconditions, which support the later failure mode, will no longer exist. Although it is such a complex process that the current simulation tools can hardly reveal the entire dynamic process, it is still a viable option that the use of combined numerical simulation and an engineering geology analysis approach will provide reasonable insight.

Based on the above four considerations, the authors believe that the possibility that the cluster No. 2 dominated the whole failure process, and triggered the secondary failure mode of cluster No. 1, is much higher than the likelihood of the other modes. The whole failure process was constituted into two closely occurring stages. In the first stage, the cluster No. 2 failed and the upper body of the Jingu landslide dramatically launched into the air and became airborne for a long distance, which resulted in a typical HSLR landslide. During the first stage, on one side, the trailing edge of the cluster No. 1 was seriously struck and scraped by the movement of the toe of rupture surface of the cluster No. 2. On the other side, the potential failure of cluster No. 1 was developing and some parts of cluster No. 1, e.g., its toe of rupture surface, had the

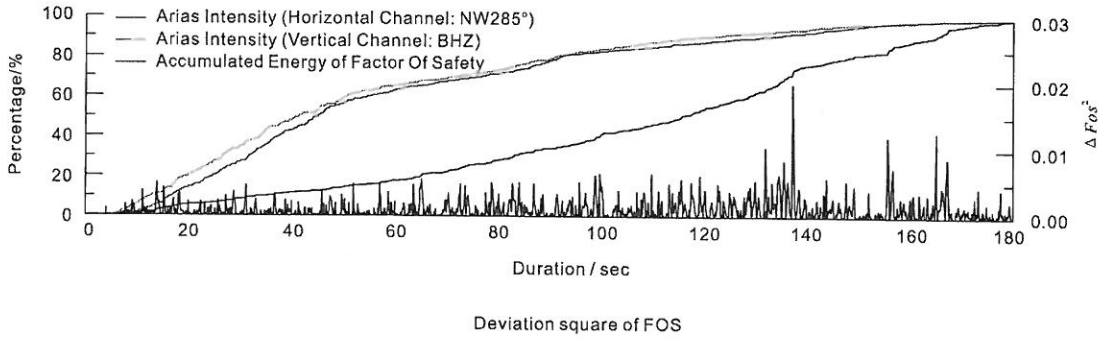

Fig. 9. Energy analysis of Jingu high-speed and long-run-out landslide in Wenchuan earthquake waveform.

possibility of failure. Therefore, in the second stage, the intrinsic factor of cluster No. 1 and the extrinsic factor from cluster No. 2 triggered a secondary failure with limited transport distance of the landslide mass. The field investigation evidence confirmed that the Jingu landslide occurred in two closely linked stages whose occurrence sequence clearly reflect the process of progressive failure at macro level.

This trigger mechanism analysis is based on the quantitative results of spatial distribution of dynamic critical slip surfaces, and is consistent with the qualitative analysis in Section 6.2.

6.3.5. Dynamic reliability analysis by the statistical window of duration

The definitions of significant durations, either for ground motion or for factor of safety, are closely related to a certain energy distribution respectively. Fig. 9 presents the Arias Intensity (e.g., Elnashai and Sarno, 2008) curves and AEF curve defined according to Eq. (7). Table 5 lists both start points and end points of the durations on different thresholds.

As shown in Fig. 9 and Table 5, the AEF curve and Arias Intensity curves do not match, which illustrates the fact that the significant duration of factor of safety has considerable difference from the significant durations of the horizontal and vertical acceleration channels. The reason behind the difference is very complex. It is widely accepted that the response of landslides always lags behind the ground motion, and the lag time is hard to deduce quantitatively. Among various factors that affect the dynamic response, the damping characteristics and natural vibration period of the landslide are the two most important factors. Low damping and long natural vibration period will result in an obvious lag. The huge scale of the Jingu landslide implies a relativity long natural vibration period and it can be understood that the AEF curve will be different from the Arias Intensity curve. Therefore, using the significant duration based on factor of safety within the statistical windows is an effective tool to closely reflect the response characteristics of the landslide.

Table 6 gives the reliability analysis results through various statistical windows based on significant durations of factor of safety. When a statistical window is applied, the reliability index drops and the probability of failure is higher. This phenomenon is reasonable because the statistical windows eliminate a large number of sampling points with factor of safety around the average level 1.031, and the dilution effect of those points would tend to drive the evaluation results to appear to be more stable than they actually are. In this case, the difference between the statistical windows and total duration (0–180 s) approach is not great, and it is mainly because the complete duration of Wenchuan earthquake wave is over 300 s and the 180 s of wave input that was used in this case is already a "refining" from the entire ground motion. Considering that the final 120 s of 300 s are characterized by a low vibration level, it can be deduced that the results using the statistical window would reveal a more obvious difference when compared with seismic duration calculated for 300 s.

Using our suggested analytical approach, the dynamic probability of failure is 16% to 17%, which clearly reveals the considerable unstable tendency of the Jingu terrain in the conditions of the Wenchuan earthquake.

6.4. Take-off speed analysis of mass ejection

The toe of the rupture surface of the cluster No. 2 has an average of 300 meters high measured from the valley bottom, and average 500 meters in horizontal distance from the center accumulation area. According to the shape of the toe of the rupture surface in Fig. 8, the initial angle between *AB* and axis *ox* is 29°, and the initial state is flat projectile motion which means the angle between initial velocity and the positive direction of axis *ox* is zero. So, in the Eq. (8), set $H = 300$ m, $x = 500$ m, $\theta = -29°$, and $\varphi = 0°$. Table 7 is the complete list of parameters of flying simulation for inverting take-off velocity.

By programming for solving the inverse problem, the take-off speed $v_0 = 57.0$ m/s of mass ejection is obtained. Specifically, by setting C_L, C_R, and G_e to zero, a certain take-off speed $v_0' = 63.9$ m/s was obtained using the same program. In this situation, the Eq. (8) is degraded into simple flat projectile motion without considering the aerodynamic effects. The fact that the value of v_0' is very close to the 64 m/s, which is deduced from simple flat projectile motion excluding air resistance, confirms the correctness of the inverse program to some extent.

The value difference between v_0 and v_0' is derived from the fact that the shape of the flying landside body as depicted in Fig. 2 can produce effects similar to an aircraft glide. Therefore, if the aerodynamic effect is taken into account, the same initial velocity will result in a much greater flight distance compared to an approach that does not consider the aerodynamic effects.

After the take-off speed is calculated, the issue of how the landslide could reach the speed of 57.0 m/s becomes clearer. From the point of view of engineering geology, it is very possible for the upper body of

Table 5
Significant duration of Jingu high-speed and long-run-out landslide in Wenchuan earthquake waveform.

Significant duration	5%–95% energy section		5%–85% energy section		5%–80% energy section	
	Start point (s)	End point (s)	Start point (s)	End point (s)	Start point (s)	End point (s)
Horizontal channel	13.46	146.72	13.46	109.40	13.46	92.16
Vertical channel	9.08	140.86	9.08	102.88	9.08	91.08
Factor of safety	18.500	167.250	18.500	156.000	18.500	147.625

Table 6
Dynamic failure probability and reliability index of Jingu high-speed and long-run-out landslide in Wenchuan earthquake waveform.

Statistical window based on duration of factor of safety	Static factor of safety	Instantaneous factor of safety				Reliability analysis	
		Mean	Standard deviation	Max	Min	Reliability index	Probability of failure
	F_s	$\overline{Fos}$	σ	Fos_{max}	Fos_{min}	β	P_f
Total energy section (0–180 s)	1.037	1.031	0.032	1.177	0.951	0.961	0.163
5%–95% AEF (18.500–167.625 s)	1.037	1.031	0.034	1.177	0.951	0.921	0.176
5%–85% AEF (18.500–156.875 s)	1.037	1.031	0.033	1.177	0.956	0.938	0.172
5%–80% AEF (18.500–151.250 s)	1.037	1.030	0.033	1.177	0.956	0.924	0.178

Note: AEF is abbreviation of "accumulated energy of factor of safety" defined by Eq. (7).

the Jingu landslide to obtain the take-off speed over 57.0 m/s mainly based on the following two reasons.

The first reason lies in the extremely low mechanical properties of the slip surfaces in cluster No. 2. During seismic activity, the reciprocating friction movement of material particles will produce a huge energy that causes local vaporization of the ground water in the landslide body in a very short period of time. Local vaporization of pore water will significantly increase pore pressure and reduce friction along the slide surface; this results in rapid deterioration of the stability of the landslide. There were three facts that support the deduction of local vaporization. First, there are conspicuous and fresh traces of high-temperature carbonization on the surface of the rock fragments, which are widely spread along the trajectory of the mass movement. This is evidence of the high-temperature that is necessary to vaporize moisture. Second, some part of the slope mass is rich in water. The adequate water content is a necessary condition for "local vaporization." Third, many surviving residents testified that a huge mist and wave of heated air was experienced during the landslide event, which is further evidence of the vaporization of water. As for the pore-pressure effect, many previous studies (e.g., Campbell, 1989; Cleary and Campbell, 1993; Ersmann, 1979; Shreve, 1968) have suggested how excess fluid pressure has reduced sliding resistance along shear surfaces in high-speed, long runout landslides.

The second reason is a consequence of the considerable length of the slip surface which as a ski ramp, provides a sufficient takeoff boost for the mass ejection. The length of the cluster No. 2 reached 500 m which is adequate to facilitate the accumulated speed over 57.0 m/s. Actually, when compared with reported take-off speed of other typical HSLR landslides, it is very possible that the Jingu landslide obtained a takeoff speed of more than 57.0 m/s on the toe of the rupture surface of the cluster No. 2.

In addition, from the perspective of energy conservation, the range of takeoff speed can be quantitatively estimated. According to the conservation of energy, when the gravitational potential energy transformed into kinetic energy, the following expression is established.

$$\frac{1}{2}(1-\xi)m{v_0}^2 = mg\Delta h$$
$$v_0 = \sqrt{2g\Delta h/(1-\xi)} \quad (10)$$

where Δh is the difference in elevation, g is the acceleration of gravity, ξ is energy loss rate ($0\% \le \xi \le 100\%$), v_0 is the takeoff speed, and m is the mass of the landslide body.

In this case, the elevation of cluster No. 2 was distributed in the 1000 to 1300 meter range with the toe of the rupture surface located in 1000 to 1050 meter range, and the trailing edge was located in the 1250–1300 meter range. Therefore, the range of Δh is between 200 and 300 m. Based on the Eq. (10), once excluding the energy losses (set $\xi = 0$), the value of v_0 is 62.6–76.7 m/s. When the inverted velocity of 57.0 m/s is used, the corresponding energy loss rate is 17%–45%. During the movement of the sliding body, this proportion of energy is converted to heat energy and eventually dissipated. For the low creep type of landslide, the energy loss rate is up to 100%. However, for the Jingu landslide, the high-speed movement makes it reasonable for the energy loss proportion to be 17%–45% which is mainly due to the aforementioned pore-pressure effect that greatly reduced resistance during the movement of the landslide body and significantly lowered the energy loss rate.

7. Conclusions

The mass ejection type of HSLR landslide is an unusual type of landslide closely associated with a strong earthquake. Because of its complexity, the quantitative–qualitative-combined techniques described in this paper are much better suited than routine evaluation methods to reveal the formation mechanism of this type of landslide, and the following conclusions have been reached:

(1) Based on the engineering geologic analysis for actual and typical cases in Wenchuan area, four prerequisites are critical to the production of mass ejection type of high-speed and long-run out landslides: high position of the toe of the rupture surface, critical height and critical inclination of slope, sufficient open space in the movement direction, and adequate take-off speed of ski-jump-like mass ejection. These four area-specific prerequisites are the commonalities for this type of landslide, and utilizing these criteria can greatly narrow the analysis targets and improve the efficiency of screening and targeting the potential landslides.
(2) A dynamic reliability analysis method which considers the feature of energy–time distribution is proposed. When the statistical windows instead of the whole duration of ground motion are applied, this site-specific quantitative analysis can yield more credible results by emphasizing the most significant time period and the failure probability of a potential target can be more accurately evaluated.
(3) With the goal of calculating the take-off speed of mass ejection, an aerodynamic inverse method was introduced and the energy-conservation-based concise method verified the reasonableness of this method. When evaluating a new landslide, several trial thrown distances can be introduced to obtain various take-off speeds, and the most reasonable among them can be selected by this method. Using this forward and inverse combined

Table 7
Flying simulation parameters of Jingu high-speed and long-run-out landslide.

Height H/m	Level flight distance X/m	Angle between wing axis and horizontal axis θ/(°)	Angle between sliding velocity and horizontal axis ϕ/(°)	Plane area of body mass A/m^2	Body mass m/kg	Air density ρ/(kg·m^{-3})
300	500	−29	0	255,394	2.86×10^{10}	1.2250

technique, the quantitative evaluation for take-off speed was achieved.

(4) This paper provides a viable solution for locating and assessing a new potential target belonging to ME-HSLR landslide. The area-specific four prerequisites are promising tools for screening and targeting the landslides, and the site-specific dynamic reliability analysis is suitable for the quantitative assessment of the possibility of failure. Finally, the forward and inverse combined technique can evaluate the take-off speed as well as airborne distance of the mass-ejection material.

Acknowledgment

The research work presented here and the preparation of this paper have been financially supported by the National Basic Research Program of China (973 Program) Grant No. 2011CB710606), the National Nature Foundation of China (NSFC; Grant No. 41102195, No. 41230637 and No. 41272309), China Postdoctoral Science Foundation (Grant No. 2012M521500 and No. 2014T70758), the Hubei Provincial Natural Science Foundation of China (Grant No. 2014CFB901), and China State Scholarship Fund (File No. 201208420293). This paper was significantly improved with the multiple rounds of aid from the anonymous reviewers. All supports are gratefully acknowledged.

References

Bommer, J.J., Martinez-Pereira, A., 1999. The effective duration of earthquake strong motion. J. Earthq. Eng. 3, 127–172. http://dx.doi.org/10.1080/13632469909350343.

Campbell, C.S., 1989. Self-lubrication for long runout landslides. J. Geol. 97, 653–665. http://dx.doi.org/10.1086/629350.

Christian, J.T., Ladd, C.C., Baecher, G.B., 1994. Reliability applied to slope stability analysis. J. Geotech. Eng. ASCE 120, 2180–2207. http://dx.doi.org/10.1061/(ASCE)0733-9410(1994)120:12(2180).

Cleary, P.W., Campbell, C.S., 1993. Self-lubrication for long runout landslides — examination by computer-simulation. J. Geophys. Res. Solid Earth 98, 21911–21924. http://dx.doi.org/10.1029/93jb02380.

Cruden, D.M., Varnes, D.J., 1996. Landslide types and processes. In: Turner, A.K., Schuster, R.L. (Eds.), Landslides: Investigation and Mitigation (National Research Council (U.S.) Transportation Research Board Special Report). Transportation Research Board, pp. 36–75.

Cui, F.P., Yin, Y.P., Hu, R.L., Yu, J.Q., 2012. Failure mechanisms of the landslides triggered by the 2008 Wenchuan earthquake, China. In: Wang, L.H., Xu, G. (Eds.), Advances in Industrial and Civil Engineering. Pts 1–4, pp. 1864–1868. http://dx.doi.org/10.4028/www.scientific.net/AMR.594-597.1864.

Dai, F.C., Lee, C.F., Ngai, Y.Y., 2002. Landslide risk assessment and management: an overview. Eng. Geol. 64, 65–87. http://dx.doi.org/10.1016/s0013-7952(01)00093-x.

Dai, F.C., Xu, C., Yao, X., Xu, L., Tu, X.B., Gong, Q.M., 2011. Spatial distribution of landslides triggered by the 2008 Ms 8.0 Wenchuan earthquake, China. J. Asian Earth Sci. 40, 883–895. http://dx.doi.org/10.1016/j.jseaes.2010.04.010.

Elnashai, A.S., Sarno, L.D., 2008. Fundamentals of Earthquake Engineering. John Wiley & Sons, Chichester, U.K.

Ersmann, T.H., 1979. Mechanisms of large landslides. Rock Mech. 12, 15–46. http://dx.doi.org/10.1007/BF01241087.

Fang, H., 2010. Study on mechanical mechanism and controlling factors of high-speed distant landslides induced by the Wenchuan earthquake. J. Catastrophol. 25, 7. http://dx.doi.org/10.3969/j.issn.1000-811X.2010.z1.026 (in Chinese).

Guo, D.P., Hamada, M., 2013. Qualitative and quantitative analysis on landslide influential factors during Wenchuan earthquake: a case study in Wenchuan County. Eng. Geol. 152, 202–209. http://dx.doi.org/10.1016/j.enggeo.2012.10.012.

Housner, G.W., 1965. Intensity of ground motion shaking near the causative fault. The 3rd World Conference on Earthquake Engineering, Auckland, New Zealand, pp. 81–94.

Huang, J.S., Griffiths, D.V., Fenton, G.A., 2010. System reliability of slopes by RFEM. Soils Found. 50, 343–353. http://dx.doi.org/10.3208/sandf.50.343.

Huang, R.Q., Pei, X.J., Fan, X.M., Zhang, W.F., Li, S.G., Li, B.L., 2012. The characteristics and failure mechanism of the largest landslide triggered by the Wenchuan earthquake, May 12, 2008, China. Landslides 9, 131–142. http://dx.doi.org/10.1007/s10346-011-0276-6.

Hungr, O., 2004. Dynamics of rapid landslides. In: Kyoji, S. (Ed.), Landslides in Progress. Springer, Heidelberg, pp. 47–57.

Jibson, R.W., 2011. Methods for assessing the stability of slopes during earthquakes — a retrospective. Eng. Geol. 122, 43–50. http://dx.doi.org/10.1016/j.enggeo.2010.09.017.

Keefer, D.K., 1984. Rock avalanches caused by earthquakes — source characteristics. Science 223, 1288–1290. http://dx.doi.org/10.1126/science.223.4642.1288.

Kulhawy, F.H., 1969. Finite Element Analysis of the Behavior of Embankments. University of California, Berkeley.

Liu, X., 2010. Research on Dynamic Response of Slope in Wenchuan Earthquake Area. (Ph.D. thesis), China University of Geosciences (Wuhan), Wuhan (in Chinese).

Liu, X., Ez Eldin, M.A.M., 2012. Case studies on equivalent issue of soil slope stability analysis methods. 4th International Conference on New Development in Rock Mechanics and Rock Engineering, Shenyang, China, 14–17 Sep., 2012, pp. 65–71.

Liu, Y.J., Hu, H.T., Bai, Z.Y., 2002a. Aerodynamic dynamic effect of large-scale and high-speed landslide. J. Southwest Jiaotong Univ. 37, 6–9. http://dx.doi.org/10.3969/j.issn.0258-2724.2002.01.002 (in Chinese).

Liu, Y.J., Hu, H.T., Bai, Z.Y., 2002b. Testing study on aerodynamics effect of large-scale and high-speed flying landslide. Chin. J. Rock Mech. Eng. 22, 784–789. http://dx.doi.org/10.3321/j.issn:1000-6915.2003.05.018 (in Chinese).

Liu, H.L., Fei, K., Gao, Y.F., 2003. Time history analysis method of slope seismic stability. Rock Soil Mech. 24, 8. http://dx.doi.org/10.3969/j.issn.1000-7598.2003.04.013 (in Chinese).

Liu, J.F., You, Y., Chen, X.C., Fan, J.R., 2010. Identification of potential sites of debris flows in the upper Min River drainage, following environmental changes caused by the Wenchuan earthquake. J. Mt. Sci. 7, 255–263. http://dx.doi.org/10.1007/s11629-010-2017-z.

Liu, X., Tang, H.M., Hu, X.L., Wang, L.Q., Liao, S.B., Zou, Z.X., 2012. Formation mechanism and dynamic stability of Jingu high-speed and long-run-out landslide. Chin. J. Rock Mech. Eng. 31, 2527–2537. http://dx.doi.org/10.3969/j.issn.1000-6915.2012.12.017 (in Chinese).

Liu, X., Tang, H.M., Xiong, C.R., 2013. Patterns, problems, and development trends of analysis methods for slope dynamic reliability. Rock Soil Mech. 34, 1217–1234 (in Chinese).

Qi, S.W., Xu, Q.A., Lan, H.X., Zhang, B., Liu, J.Y., 2010. Spatial distribution analysis of landslides triggered by 2008.5.12 Wenchuan Earthquake, China. Eng. Geol. 116, 95–108. http://dx.doi.org/10.1016/j.enggeo.2010.07.011.

Qi, S.W., Xu, Q., Lan, H.X., Zhang, B., Liu, J.Y., 2012. Resonance effect existence or not for landslides triggered by 2008 Wenchuan earthquake: a reply to the comment by Drs. Xu Chong and Xu Xiwei. Eng. Geol. 151, 128–130. http://dx.doi.org/10.1016/j.enggeo.2012.08.003.

Shreve, R.L., 1968. Leakage and fluidization in air-layer lubricated avalanches. Geol. Soc. Am. Bull. 79, 653–658.

Tang, H.M., Jia, H.B., Hu, X.L., Li, D.W., Xiong, C.R., 2010. Characteristics of landslides induced by the Great Wenchuan Earthquake. J. Earth Sci. 21, 104–113. http://dx.doi.org/10.1007/s12583-010-0008-1.

Tang, C., Zhu, J., Qi, X., 2011a. Landslide hazard assessment of the 2008 Wenchuan earthquake: a case study in Beichuan area. Can. Geotech. J. 48, 128–145. http://dx.doi.org/10.1139/t10-059.

Tang, C., Zhu, J., Qi, X., Ding, J., 2011b. Landslides induced by the Wenchuan earthquake and the subsequent strong rainfall event: a case study in the Beichuan area of China. Eng. Geol. 122, 22–33. http://dx.doi.org/10.1016/j.enggeo.2011.03.013.

Varnes, D.J., 1978. Slope movement types and processes. In: Schuster, R.L., Krizek, R.J. (Eds.), Landslides: analysis and control (special report — Transportation Research Board, National Research Council, No. 176). Transportation Research Board, pp. 11–33.

Wang, Z.H., 2008. A thunder at the beginning of the 21st century — the giant Yigong landslide. Landslides and Engineered Slopes: From the Past to the Future vols. 1 and 2, pp. 2111–2118.

Wang, F.W., Sun, P., Konagai, K., Cheng, Q.G., Yin, Y.P., Fukuoka, H., 2009. The mechanism of initiation and motion of the rapid and long runout landslides striggered by the 2008 Wenchuan earthquak. In: Liang, W.H., Li, Q., Gao, B. (Eds.), Proceedings of International Conference on Earthquake Engineering - the First Anniversary of Wenchuan Earthquake, pp. 723–728.

Wang, G.H., Huang, R.Q., Kamai, T., Zhang, F.Y., 2013. The internal structure of a rockslide dam induced by the 2008 Wenchuan (M(w)7.9) earthquake, China. Eng. Geol. 156, 28–36. http://dx.doi.org/10.1016/j.enggeo.2013.01.004.

Wasowski, J., Keefer, D.K., Lee, C.T., 2011. Toward the next generation of research on earthquake-induced landslides: current issues and future challenges. Eng. Geol. 122, 1–8. http://dx.doi.org/10.1016/j.enggeo.2011.06.001.

Wu, S.R., Wang, T., Shi, L., Sun, P., Shi, J.S., Li, B., P., X., Wang, H.B., 2010. Study on catastrophic landslides triggered by 2008 great Wenchuan earthquake, Sichuan, China. J. Eng. Geol. 18, 15. http://dx.doi.org/10.3969/j.issn.1004-9665.2010.02.001.

Wu, Z.H., Barosh, P.J., Zhang, Z.C., Liao, H.J., 2012. Effects from the Wenchuan Earthquake and seismic hazard in the Longmenshan Mountains at the eastern margin of the Tibetan Plateau. Eng. Geol. 143, 28–36. http://dx.doi.org/10.1016/j.enggeo.2012.06.006.

Xu, B., Low, B.K., 2006. Probabilistic stability analyses of embankments based on finite-element method. J. Geotech. Geoenviron. Eng. 132, 1444–1454. http://dx.doi.org/10.1061/(Asce)1090-0241.

Xu, C., Xu, X.W., 2012. Comment on "Spatial distribution analysis of landslides triggered by 2008.5.12 Wenchuan Earthquake, China" by Shengwen Qi, Qiang Xu, Hengxing Lan, Bing Zhang, Jianyou Liu [Engineering Geology 116 (2010) 95–108]. Eng. Geol. 133, 40–42. http://dx.doi.org/10.1016/j.enggeo.2012.02.017.

Yin, Y.P., 2009. Rapid and long run-out features of landslides triggered by the Wenchuan earthquake. J. Eng. Geol. 17, 14. http://dx.doi.org/10.3969/j.issn.1004-9665.2009.02.002 (in Chinese).

Yin, Y.P., Wang, F.W., Sun, P., 2009. Landslide hazards triggered by the 2008 Wenchuan earthquake, Sichuan, China. Landslides 6, 139–152. http://dx.doi.org/10.1007/s10346-009-0148-5.

Yin, Y.P., Zheng, W.M., Li, X.C., Sun, P., Li, B., 2011. Catastrophic landslides associated with the M8.0 Wenchuan earthquake. Bull. Eng. Geol. Environ. 70, 15–32. http://dx.doi.org/10.1007/s10064-010-0334-7.

Zhao, A.P., Feng, C., Li, S.H., Ai, C., Liu, Y., 2012. Experimental research on seismic failure mode and supporting for slope of bedrock and overburden layer. Rock Soil Mech. 33, 515–523. http://dx.doi.org/10.3969/j.issn.1000-7598.2012.02.031 (in Chinese).

Zheng, H., Liu, D.F., Li, C.G., 2005. Slope stability analysis based on elasto-plastic finite element method. Int. J. Numer. Methods Eng. 64, 1871–1888. http://dx.doi.org/10.1002/nme.1406.